JOURNAL OF MATERIALS SCIENCE **35** (2000) 1051–1064

The effects of Al and Si additions on the microstructures of precipitates in low carbon steels containing Sn

X. LI, A. WATSON, R. BRYDSON, A. JHA, R. C. COCHRANE
Department of Materials, School of Process, Environmental and Materials Engineering, University of Leeds, Leeds LS2 9JT
E-mail: a.watson@leeds.ac.uk

The microstructures of low carbon steels with Sn additions were investigated using scanning electron microscopy, electron probe microanalysis, transmission electron microscopy and energy dispersive X-ray spectroscopy. Four steels based on Fe-0.9Nb-0.3Sn-0.05C (wt%) with different levels of Al and Si additions were prepared by arc melting under an argon atmosphere. The effects of heat treatment and the level of alloying elements Al and Si on the precipitation of Sn-rich phases were studied. After ageing at 1150°C and 850°C, NbC precipitates were found in all samples, as well as AlN in the higher Al content steels. The concentration of Al in steel was also found to affect the formation of Sn-rich compounds after heat treatment at 850°C for 96 hours. In the lower Al or Al-free steels, a η-Fe_2Nb_3 phase, which dissolves a significant amount of Si, was observed. In the higher Al steels, a Fe_2Nb-based Laves phase, which dissolves both Si and Sn was detected. A mechanism based on both size factors and thermodynamic considerations is described, which accounts for the experimental observations.

1. Introduction

The recycling of steel scrap is becoming increasingly important for environmental considerations [1]. The current UK target is to recycle up to 250,000 tonnes of tin-can scrap per year by the year 2001. As a result, the tin content of the steel will rise to higher levels, resulting in the grain boundary segregation of elemental Sn [1, 2]. Recent evidence [3] suggests that the formability and mechanical properties of deep drawing steels will be compromised should the Sn content reach or exceed 0.05 wt %. No economic method currently exists for the removal of Sn during steelmaking and existing detinning plants have limited capacity. Environmental considerations may also place constraints to the expansion of detinning capacity. However, if Sn can be precipitated in an innocuous form, such as an intragranular intermetallic phase, then this may be one way of coping with increasing Sn additions which might be expected in the future.

At present, Al cans are recycled separately from steel cans at source as no particular advantage is gained by using the Al in the course of steelmaking. If Sn-rich compounds can be formed by deliberate additions of aluminium to steel, then mixed loads of scrap could be used with a saving in the costs of sorting scrap prior to use, provided of course the steel has useable properties.

Of the possible alloying strategies, those based on the formation of stable intermetallic phases seem most appropriate. For example, both Al and Ti form stable intermetallic compounds with Fe as does Nb. Whilst the maximum solubility of Al and Ti in α-Fe is about 35 wt% and 10 wt% respectively, that of Nb is 1.2 wt% [4]. Accordingly, a rather higher amount of Al and Ti is required to produce intermetallic compounds compared with Nb. In addition, Nb is known to form a stable phase with Sn, Nb_3Sn. It seems reasonable, therefore, that a first attempt at 'chelating' Sn in α-Fe could exploit the propensity of Nb to combine with both Sn and Fe. Although the levels required are well in excess of what would be needed in Nb microalloyed steels, as an indication that the principles were correct the Fe-Nb-Sn system could be considered as a model system.

Previous studies of Fe-Nb alloys by the authors have indicated that Sn is accommodated in the Laves (Fe_2Nb) phase in Fe-0.9Nb alloys [5]. This result is encouraging as it suggests that provided the Laves phase is formed, then Sn could be preferentially precipitated within it removing the deleterious effects arising when Sn segregated to grain boundaries. Whether this is the case in low carbon steels is unknown since the presence of other alloying elements will affect the stability of any intermetallic compounds relative to carbides.

The aim of the present work was twofold. Firstly, to examine the precipitate microstructure in the low carbon steels corresponding to the alloys investigated previously and secondly, to investigate the effects of Al and Si on the stability of the Sn-precipitation. In this paper, the results are presented in terms of the morphology, crystal structure and composition of the precipitates observed by a wide range of techniques, such as scanning

TABLE I Target composition of steels prepared (wt%)

Alloy	C	Si	Mn	Al	Sn	Nb
S1	0.05	0.3	0.64	0.03	0.3	0.9
S2	0.053	0.34	0.64	1.97	0.3	0.9
S3	0.065	0.024	0.74	2.045	0.3	0.9
S4	0.061	0.022	0.046	∼	0.3	0.9

'∼' indicates the corresponding values are too low to be statistically significant.

electron microscopy (SEM), electron probe microanalysis (EPMA), transmission electron microscopy (TEM) and energy dispersive X-ray spectroscopy (EDX). Thermodynamic calculations were carried out and compared with the experimental observations.

2. Experimental procedures

2.1. Materials

Four alloys with different levels of Al and Si were prepared by arc melting under an argon atmosphere. Repeated melting of the alloys was performed to ensure macroscopic homogeneity of the cast material. The target chemical compositions (in wt%) of the steels used in this study are listed in Table I. Here, the contents of Nb and Sn were kept at the same levels as those in the Fe alloys studied previously [5]. Although chemical analysis for nitrogen and oxygen content of the alloys was not undertaken their levels were estimated to be 150 and 100 ppm respectively from previous work. The Mn content in alloy S4 and the Si content in alloy S3 and alloy S4 were calculated from the composition of the high carbon steel used in the preparation of the alloys.

After melting, all alloys were first cold rolled to approximately 50% of the starting thickness and sealed in silica tubes under a reduced pressure (0.2 atm) of argon to minimise oxidation. The samples were heat treated at 850°C for 96 hours or 1150°C for 1 hour, followed by air cooling. The heat treatments used were the same as used previously [5], the expectation being that during heat treatment at the higher temperature the material would be in the austenitic region, whereas the material heat treated at the lower temperature would be processed in the ferritic range.

2.2. Metallography

The as-cast structure of the remelted button indicated no major segregation. The overall microstructures of the steels following the different heat treatment conditions were determined using standard metallographic procedures. SEM, in back scattered electron imaging mode, was used as a first step to examine the microstructure. This technique can emphasise the compositional differences between the various phases present. Linescans of the various elements were performed using conventional electron probe microanalysis which allowed detection of very small concentrations of each element as well as giving the elemental distribution within the particles.

TEM techniques were used to characterise the precipitates present in all alloys. Thin foil specimens were prepared by twin jet electro-polishing using a solution of 300 ml ethanol, 150 ml 2-butoxyethanol and 50 ml (60%) perchloric acid. The polishing temperature was around −10°C at a voltage of 15 V. The electron microscope employed was a Philips CM 20 TEM operated at 200 kV and equipped with an ultra thin window energy dispersive X-ray spectrometer (EDX) system (Oxford Instruments). Whilst performing microanalysis, the specimen was held in a low background beryllium holder tilted 15 from the normal towards the detector. The X-ray count rate was optimised at about 1500–2000 counts s^{-1} over 100 seconds. The data were acquired and analysed using a Link QX2000 system and the RTS-2/FLS program for thin foil microanalysis. This program corrects the data for atomic number and absorption effects and takes into account the overlapping of peaks by fitting the spectra to standard profiles. K factors for calibration of the EDX spectra were taken from the virtual standards supplied with the software.

3. Results

The microstructures of alloy S1 and alloy S2 aged at 850°C and 1150°C are shown in Figs 1 and 2 respectively. They show that precipitates appeared in all samples and were mainly distributed along grain boundaries. For both alloys, the density of the precipitates at 1150°C (Figs 1b and 2b) is lower than that at 850°C (Figs 1a and 2a). The higher Al containing samples also show more precipitates than those with lower Al compositions. As differing contrast in back scattered electron images indicates differences in composition, Fig. 2 also reveals that there is a phase which is darker than the matrix and therefore richer in the low atomic number elements. Similar microstructures were also observed in the alloy S3 (high Al) and alloy S4 (Al free). Details of the nature of these phases will be described later in this section.

For the lower Al containing steel (Alloy S1) aged at 850°C, EPMA line scans of C, Nb, Si and Sn (Fig. 3a–d) across two types of precipitates revealed that the larger precipitate was enriched in Nb and Si, while the smaller precipitates were enriched only in C and Nb. Sn was not detected in either type of precipitate. For the higher Al containing steel (S2) aged at 850°C, the line scan analyses of the same elements (Fig. 4a–d) indicate that one type of bright precipitate was similar to that in the previous sample, i.e. in that it contained C and Nb. In addition to the enrichment of Nb and Si, the other type of precipitate, also contained Sn, albeit at a low level.

Fig. 5a–d are the EPMA line scans of C, Nb, N and Al across the dark precipitates in the higher Al steel (S2) which revealed that these particles were enriched in N and Al. Adjacent to the large dark AlN particles are smaller precipitates enriched in Nb and C. It appears that NbC had nucleated on the surface of the AlN particles, which was subsequently confirmed in the TEM observation.

After ageing at 1150°C, the C and Nb rich precipitates were found in all samples, however, AlN was still only observed in high Al content steels.

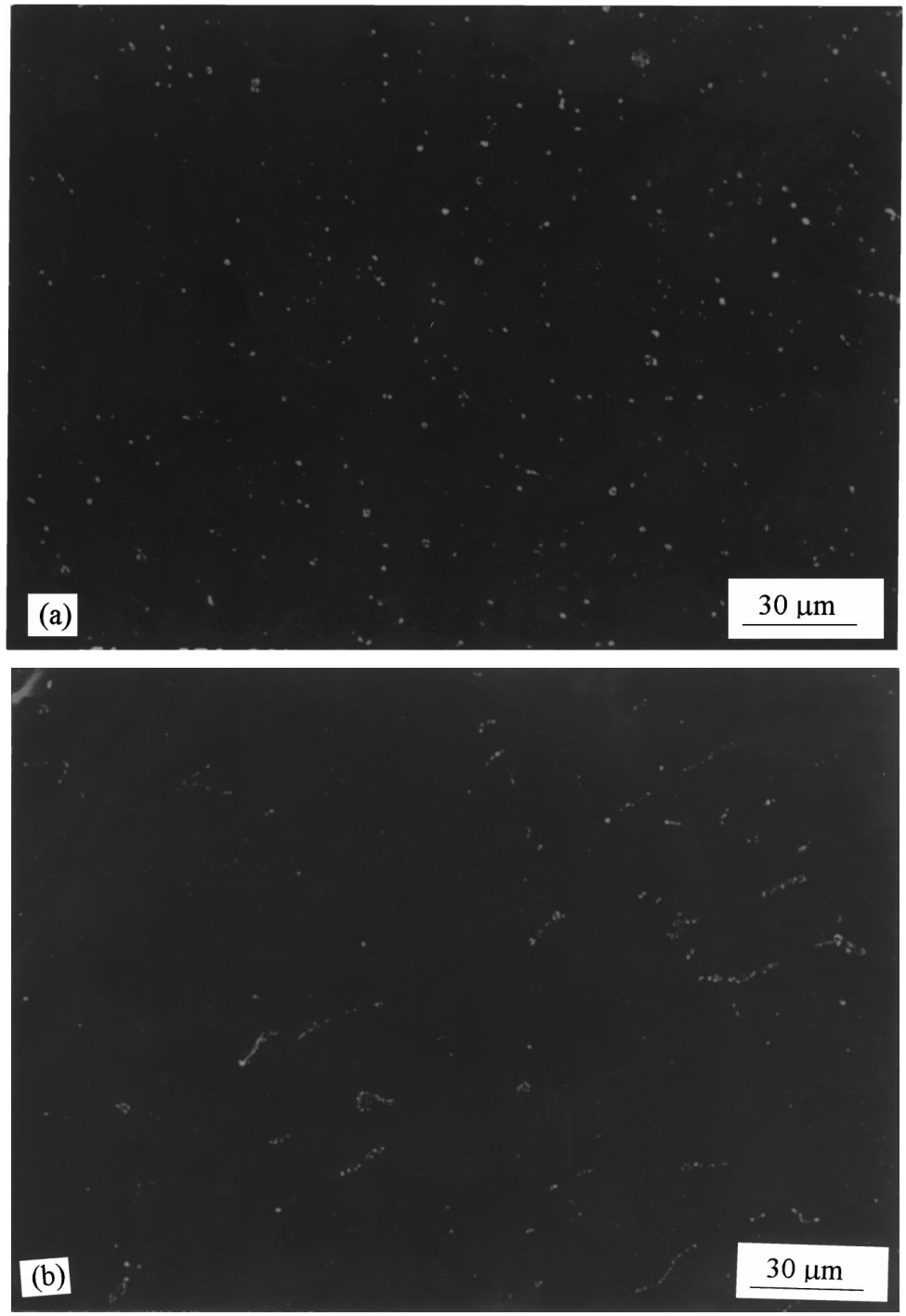

Figure 1 SEM micrographs of the steel S1: (a) 850°C for 96 hours and (b) 1150°C for 1 hour.

Further analysis of the microstructures of the precipitates was carried out using selected-area diffraction (SAD) in the TEM. Fig. 6a is a typical TEM micrograph of the C and Nb-rich phase present in the lower Al steel aged at 1150°C. From the statistical results of more than ten different observations, the particles were found to be 0.1–1 μm in diameter and ranging from near spherical to elliptical in morphology. A typical SAD pattern from this type of precipitate is shown in Fig. 6b, and is consistent with the NbC phase which has an f.c.c. crystal structure with a lattice parameter of $a = 0.447$ nm [6]. By combining the results from SEM and EPMA, it can be concluded that the C and Nb enriched phase observed in all samples is the cubic monocarbide NbC.

Fig. 7a is a bright field TEM micrograph of the lower Al containing sample aged at 850°C. SAD patterns and EDX analyses obtained from the precipitates are consistent with the η-Fe_2Nb_3 phase which has an f.c.c. crystal structure with a lattice parameter of $a = 1.126$ nm [7]. This type of particle normally adopts an irregular shape and has a size of about 1 to 5 μm, and grain boundary η-Fe_2Nb_3 particles have also been found. A typical SAD pattern of this type of precipitate is shown in Fig. 7b, which is from a zone axis of $[\bar{1}11]_\eta$.

The microstructure of Nb, Si and Sn rich precipitates in the higher Al steel aged at 850°C is shown in Fig. 8a. This micrograph is taken from the grain boundary region. A typical SAD pattern, which is consistent

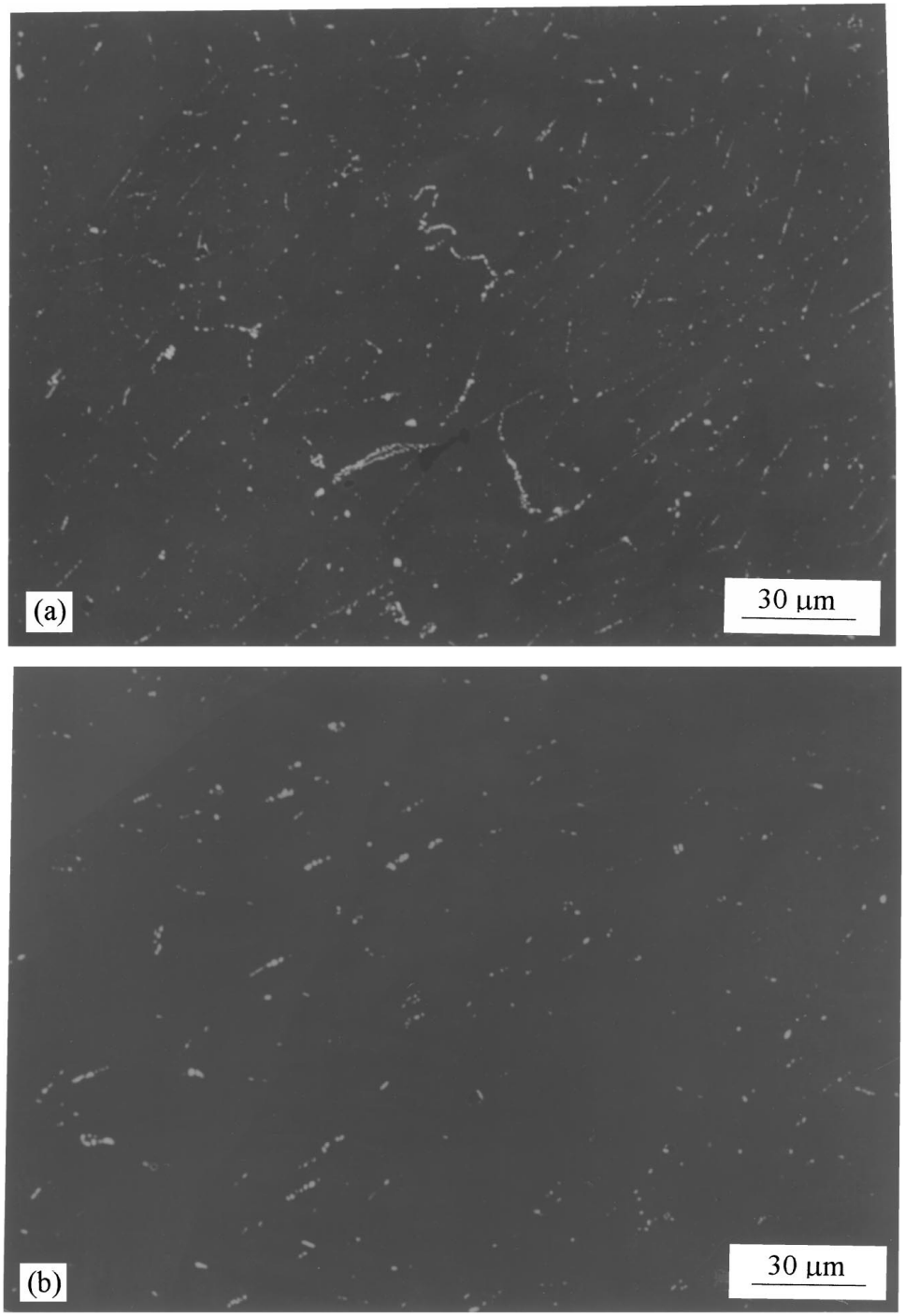

Figure 2 SEM micrographs of the steel S2: (a) 850°C for 96 hours and (b) 1150°C for 1 hour.

with the Fe_2Nb-Laves phase having a hexagonal crystal structure and lattice parameters of $a = 0.4830$ nm and $c = 0.7879$ nm [7], is shown in Fig. 8b. The size of the Laves phase particles varied from 0.2 to 2 μm. It has been observed that some Laves phase particles contained fine striations and the SAD patterns taken from them contained many streaks which were perpendicular to the fine striations suggesting a faulted structure [8].

Fig. 9a shows a bright field micrograph of a precipitate in the higher Al steel aged at 850°C. This type of particle was found to be about 3–4 μm in diameter adopting a polygonal shape. The large Al and N rich particles were randomly distributed in the matrix and were considered to be formed during solidification. However, these particles were found only occasionally in the TEM foils. Also this particle is normally much thicker than the adjacent matrix region within the foils and, therefore, it was difficult to produce diffraction patterns and accurate EDX analyses. To solve this problem, ion beam thinning was used to further thin the TEM foil, and SAD and EDX analyses were carried out in the thinnest areas of the samples very close to the electro-polishing hole. A typical SAD pattern from this large type of precipitate is given in Fig. 9b which is consistent with AlN with an hexagonal crystal structure and lattice parameters of $a = 3.11$ nm and $c = 4.98$ nm [6]. It should also be noted (shown in Fig. 9a) that there is a cluster of NbC particles nucleated on this coarse AlN particle.

TEM examinations were also carried out for alloys S3 and alloy S4 and a summary of the observations is given in Table II showing the difference between the

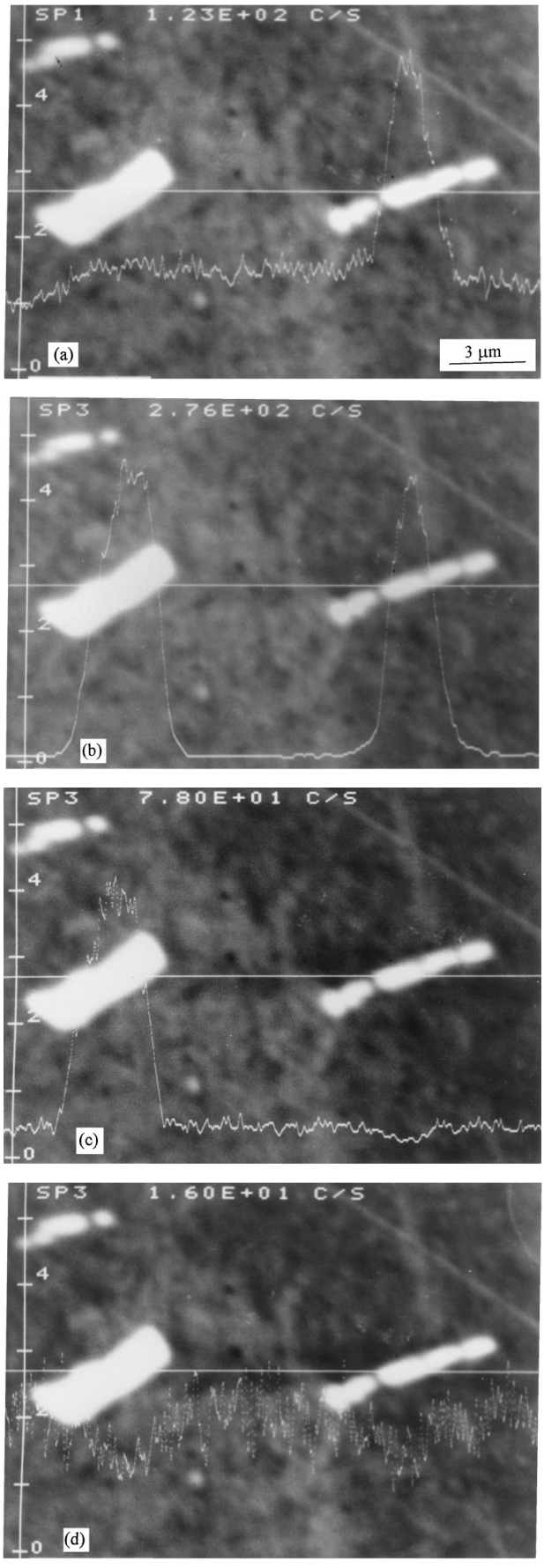

Figure 3 EPMA line scan analyses across precipitates in steel S1 after ageing at 850°C for 96 hours showing the larger precipitate is rich in Nb and Si and the smaller precipitate contains C and Nb. Sn was not detected in either type of precipitate: (a) Line scan of C, (b) Line scan of Nb, (c) Line scan of Si and (d) Line scan of Sn.

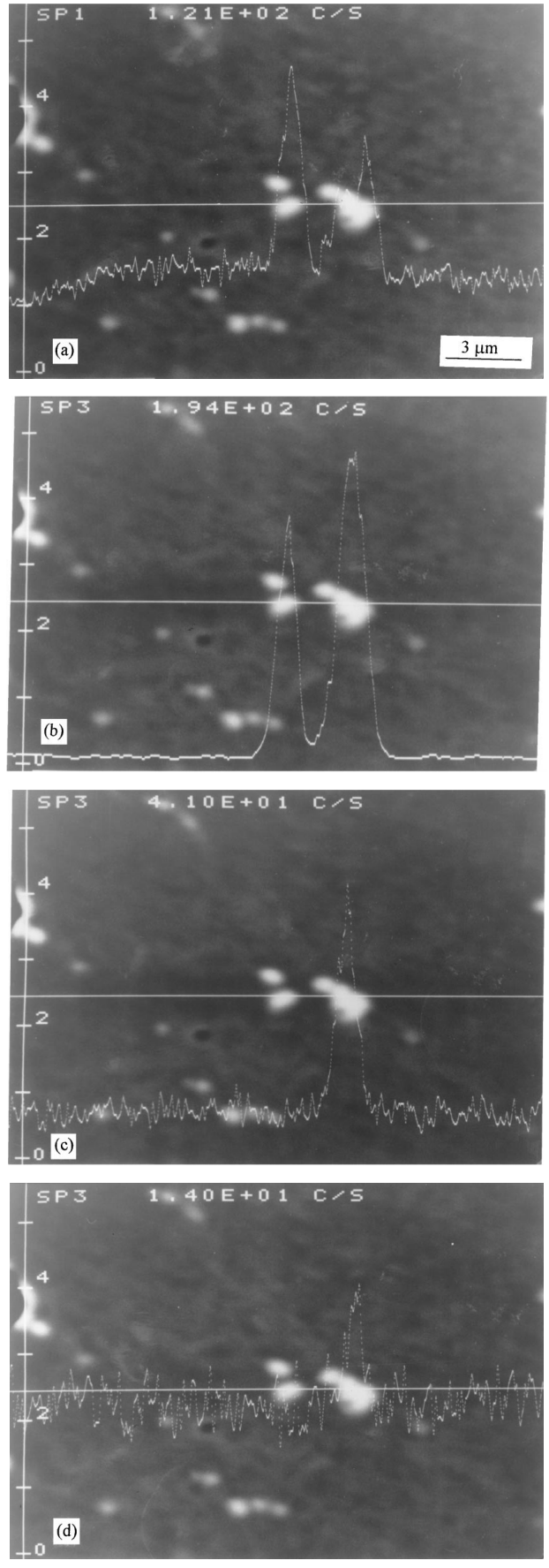

Figure 4 EPMA line scan analyses across precipitates in steel S2 after ageing at 850°C for 96 hours showing one type precipitate is rich in C and Nb and the other type of precipitate contains Nb, Si and Sn: (a) Line scan of C, (b) Line scan of Nb, (c) Line scan of Si and (d) Line scan of Sn.

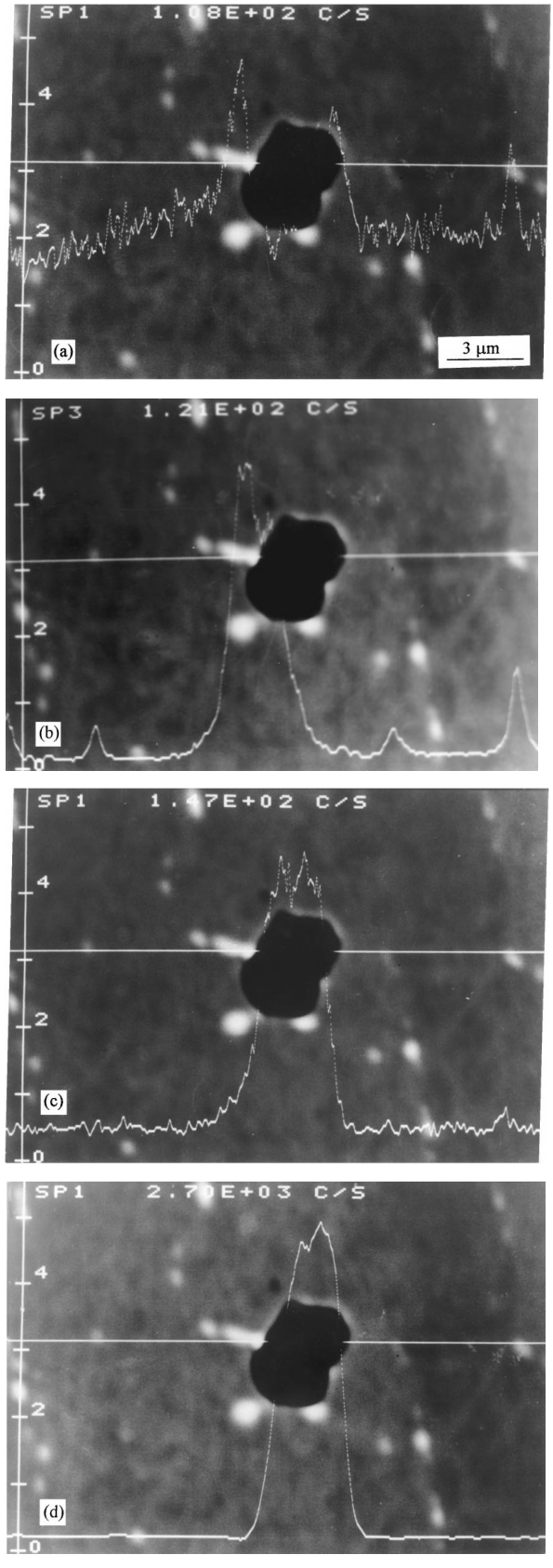

Figure 5 EPMA line scan analyses across precipitates in steel S2 after ageing at 850°C for 96 hours showing the dark precipitate, which is rich in N and Al, co-existing with C and Nb rich particles: (a) Line scan of C, (b) Line scan of Nb, (c) Line scan of N and (d) Line scan of Al.

phases observed in the four steels. It can be seen from this table that the Sn-rich Laves phase occurred in the two higher Al-containing alloys (S2 and S3) but did not appear in the lower Al (S1) and Al-free (S4) steels

TABLE II Precipitates observed after ageing under given conditions

Materials	1 hour at 1150°C	96 hours at 850°C
S1	NbC	NbC, η-Fe_2Nb_3
S2	NbC, AlN	NbC, AlN, Laves-Fe_2Nb
S3	NbC, AlN	NbC, AlN, Laves-Fe_2Nb
S4	NbC	NbC, η-Fe_2Nb_3

TABLE III Compositions of the Nb-rich precipitates obtained by EDX in TEM (wt%)

Alloys	Phase	Fe	Nb	Al	Mn	Si	Sn
S1	Matrix	98.30	0.56	∼	0.59	0.34	0.35
	Fe_2Nb_3	29.64	66.86	∼	0.20	3.64	∼
S2	Matrix	96.71	0.23	2.02	0.47	0.36	0.21
	Fe_2Nb	47.07	46.73	0.33	0.46	3.94	1.46
S3	Matrix	96.46	0.51	2.04	0.68	∼	0.13
	Fe_2Nb	50.92	43.52	0.43	0.55	1.14	3.47
S4	Matrix	98.38	0.57	∼	∼	∼	0.23
	Fe_2Nb_3	37.26	62.41	∼	∼	0.34	∼

'∼' indicates the corresponding values are too low to be statistically significant.

in which the metastable η-Fe_2Nb_3 phase was found. The average of over five quantitative EDX analyses (in wt%) for Nb-rich precipitates in the four steels aged at 850°C is given in Table III.

It can be seen from Table III that the η-Fe_2Nb_3 phase contained the elements of Fe, Nb and Si while the Fe_2Nb-Laves phase contained the elements Fe, Nb, Si and, most importantly, Sn. This result is consistent with the above EPMA observations. The levels of the elements in the Laves phase and the η-Fe_2Nb_3 phase varied due to the different matrix compositions. This will be discussed later.

It should be pointed out that as the concentration of Al in the Laves phase is significantly lower than in the matrix this suggests that the Laves phase is deficient in Al and essentially Al-free. Also, as the level of Mn in both types of precipitates are of the same order as in the corresponding matrix, the change in the precipitate compositions is mainly due to the change in the content of Fe, Nb, Si and Sn of the alloy.

4. Discussion

4.1. Precipitation of AlN and NbC

The phases identified are largely as expected on thermodynamic grounds. The presence of AlN and NbC follows from their relative solubilities in the Fe-rich matrix. Thermodynamic calculations suggest that for the alloys studied at 1150°C and 850°C there are would be .52 (at 1150°C) and .47 (at 850 °C) wt%Nb, and .003 wt %Al precipitated as NbC and AlN respectively. AlN is predicted to be stable in alloys with high Al additions. Several instances of co-precipitation of microalloy carbides and/or nitrides have been reported elsewhere [9]. Consequently, in view of the aluminium content, observations of NbC precipitating on existing AlN is consistent with previous observations.

Many of the precipitates shown in Figs 1 and 2 appear to be aligned, suggesting they have nucleated on

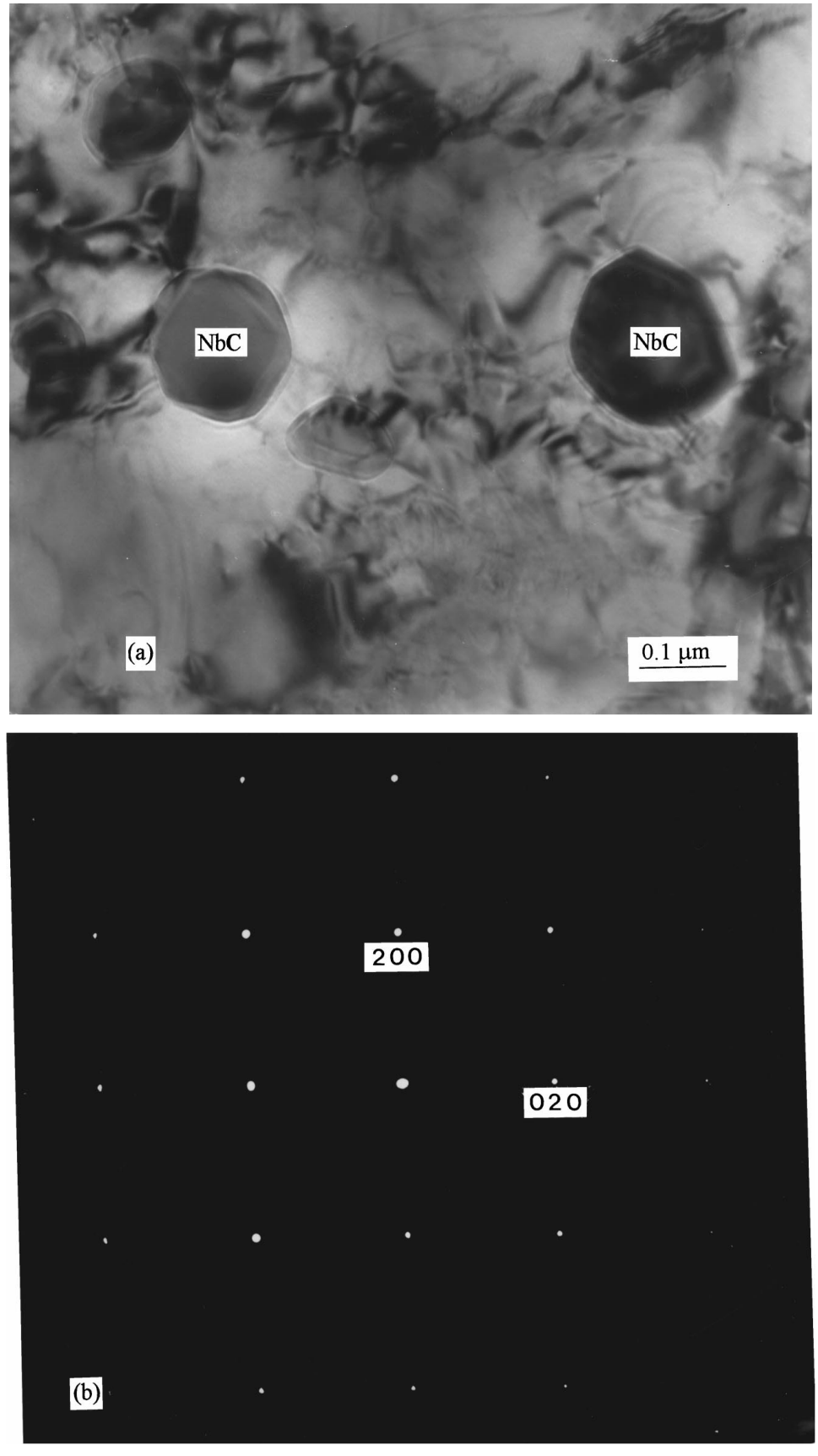

Figure 6 NbC formed in steel S1 after the ageing at 1150°C for 1 hour: (a) bright field image and (b) SAD pattern of NbC from zone axis of [001].

previous grain boundaries which would have had a higher energy and greater atomic disorder than the grain interiors. For all alloys, the microstructure of the matrix after heat treatment at 1150°C and 850°C followed by air-cooling was bcc ferrite. However, the number density of the precipitates after heat treatment at 1150°C is lower than that at 850°C. This is due to the precipitation of the Nb-intermetallic which is soluble at the higher temperature. At both temperatures, the number density of the precipitates in the higher Al containing steel is higher than that in the lower Al composition material. This is due to the precipitation of AlN. As shown in

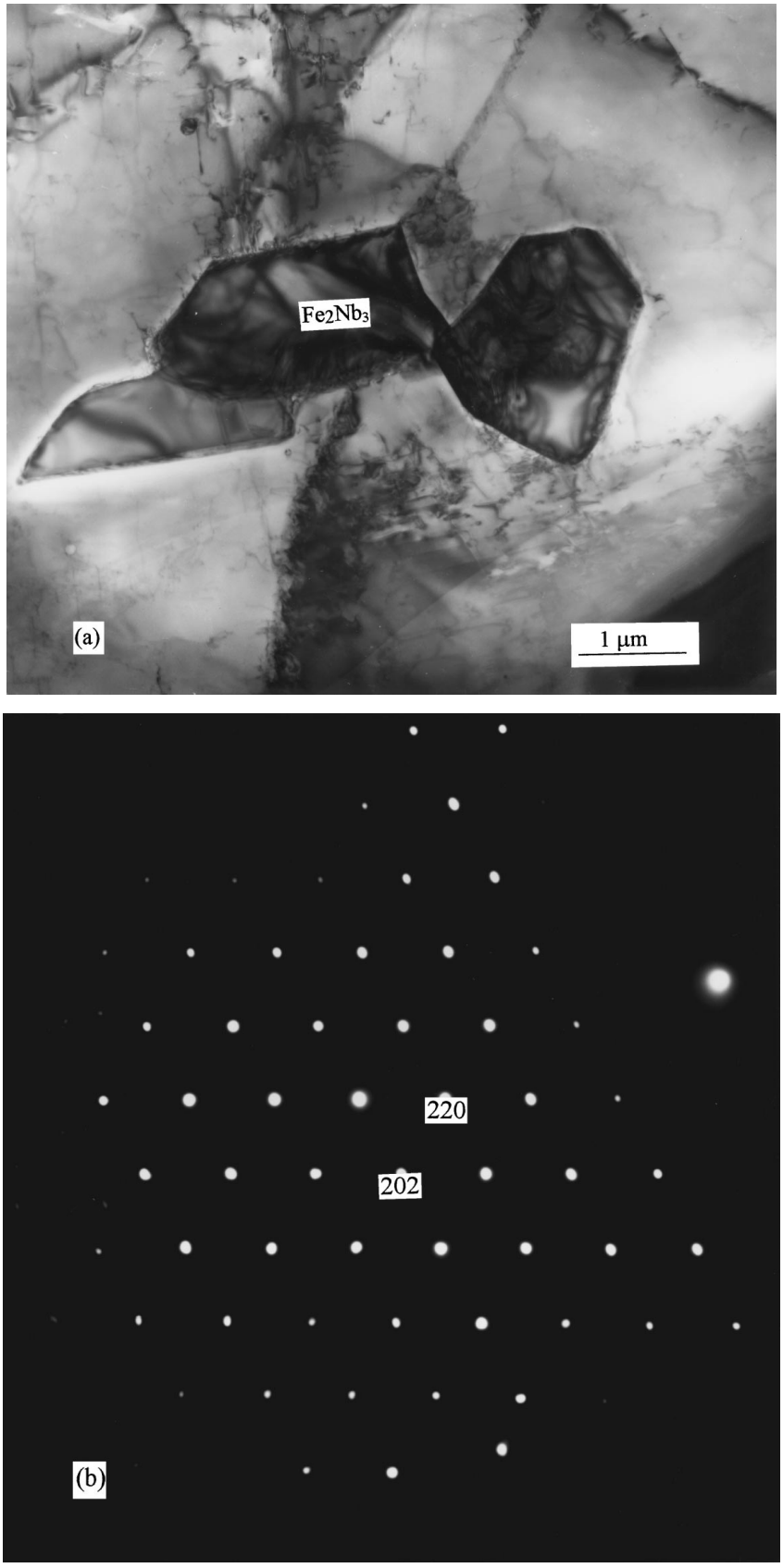

Figure 7 η-Fe_2Nb_3 phase formed in the lower Al steel S1 after ageing at 850°C for 96 hours: (a) bright field image and (b) SAD pattern from zone axis of $[\bar{1}11]_\eta$.

Figs 5 and 9, the AlN particles are much larger than the NbC particles which appear to have precipitated heterogeneously on the surface of the AlN particles suggesting that AlN aids nucleation of the carbide precipitates by providing favourable sites.

4.2. Precipitation of intermetallic phases

After ageing at 850°C, the intermetallic η-Fe_2Nb_3 and Fe_2Nb-Laves phases were found in the low (or Al-free) and high Al-content alloys respectively. It has been reported that the η-Fe_2Nb_3 phase is not stable in the Fe-Nb

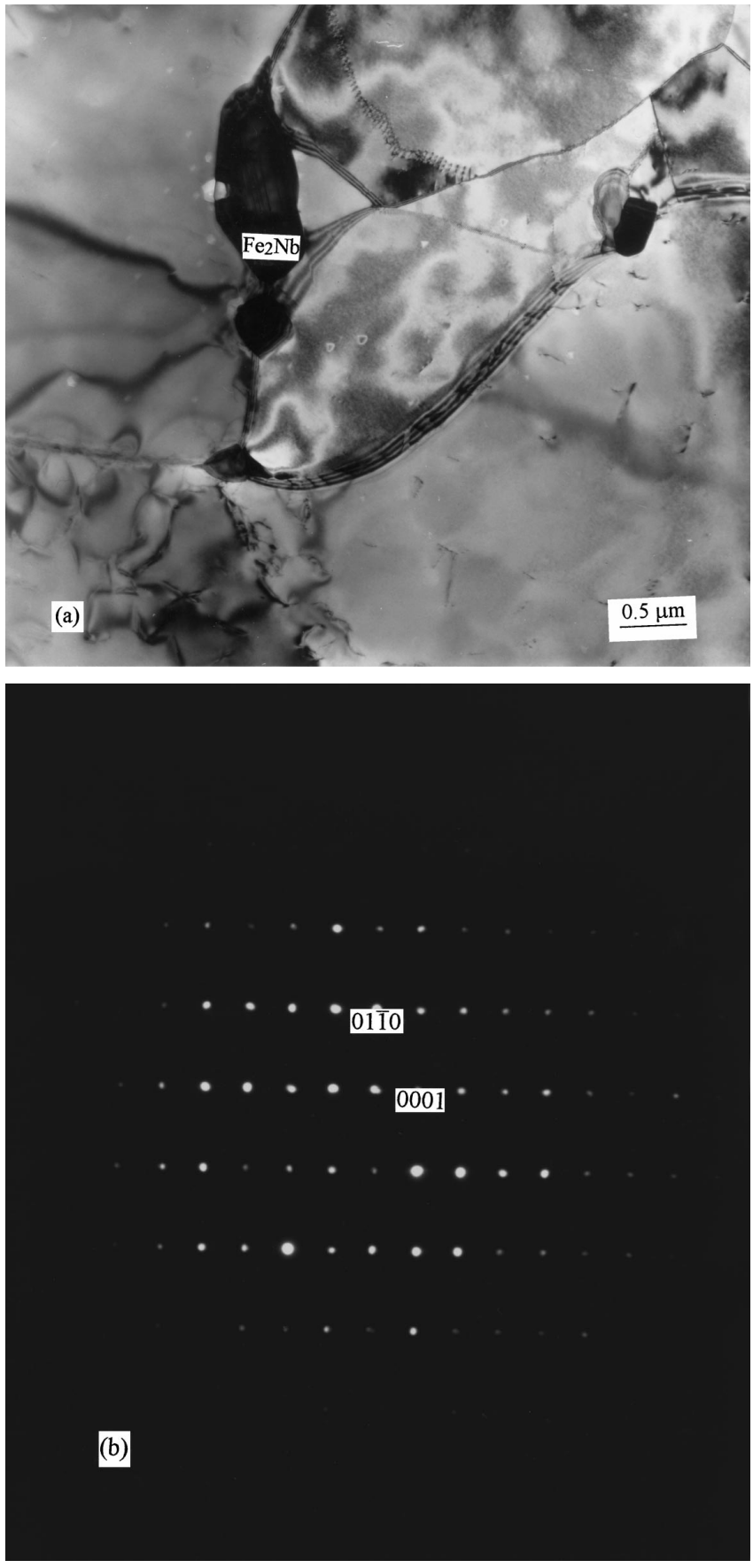

Figure 8 Fe_2Nb-Laves phase formed in the higher Al steel after ageing at 850°C for 96 hours: (a) bright field image and (b) SAD pattern of Fe_2Nb-Laves phase from zone axis of [2$\bar{1}$10].

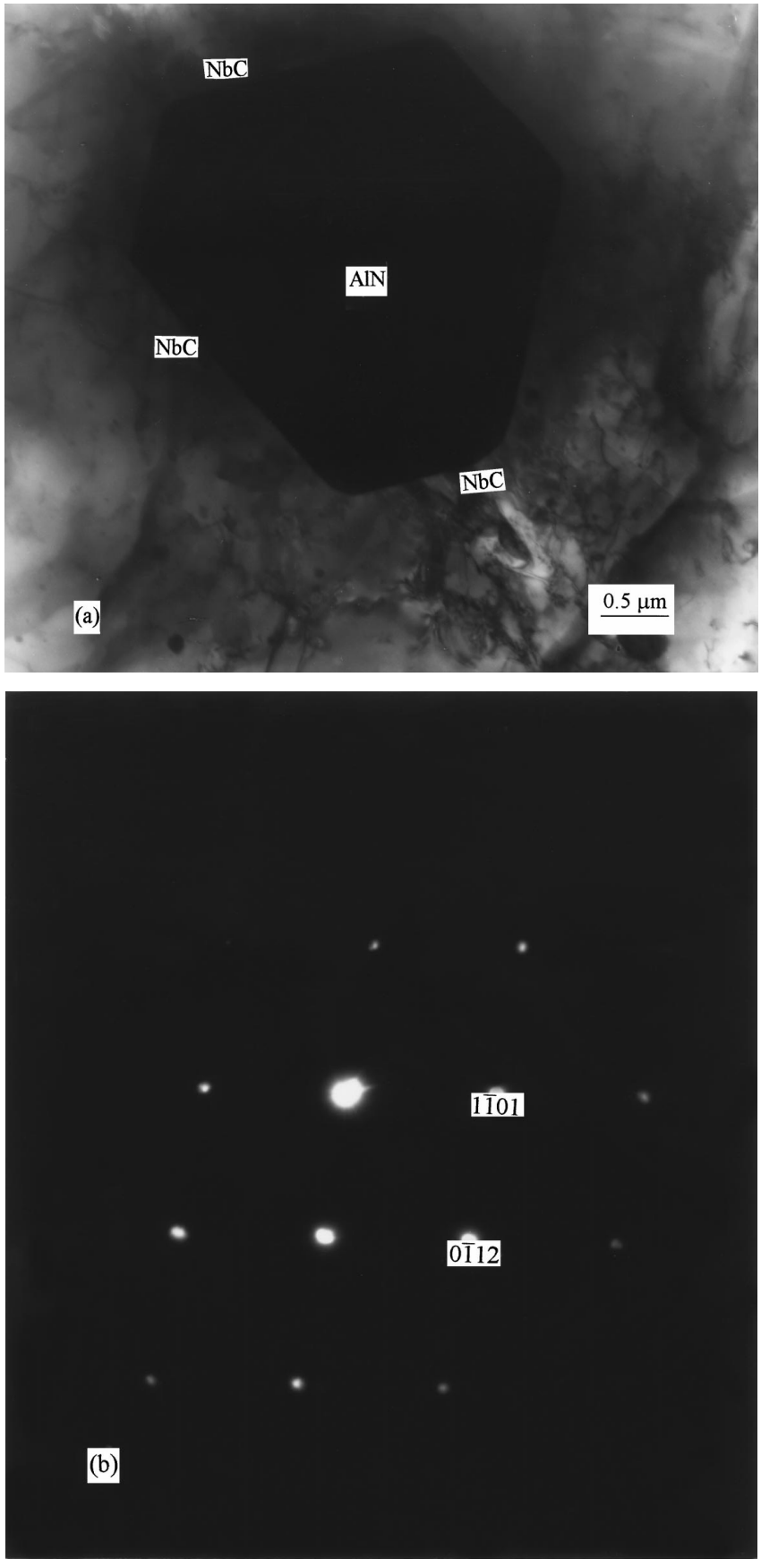

Figure 9 AlN formed in the higher Al steel after ageing at 850°C for 96 hours: (a) bright field image and (b) SAD pattern of AlN from zone axis of [01$\bar{1}\bar{1}$].

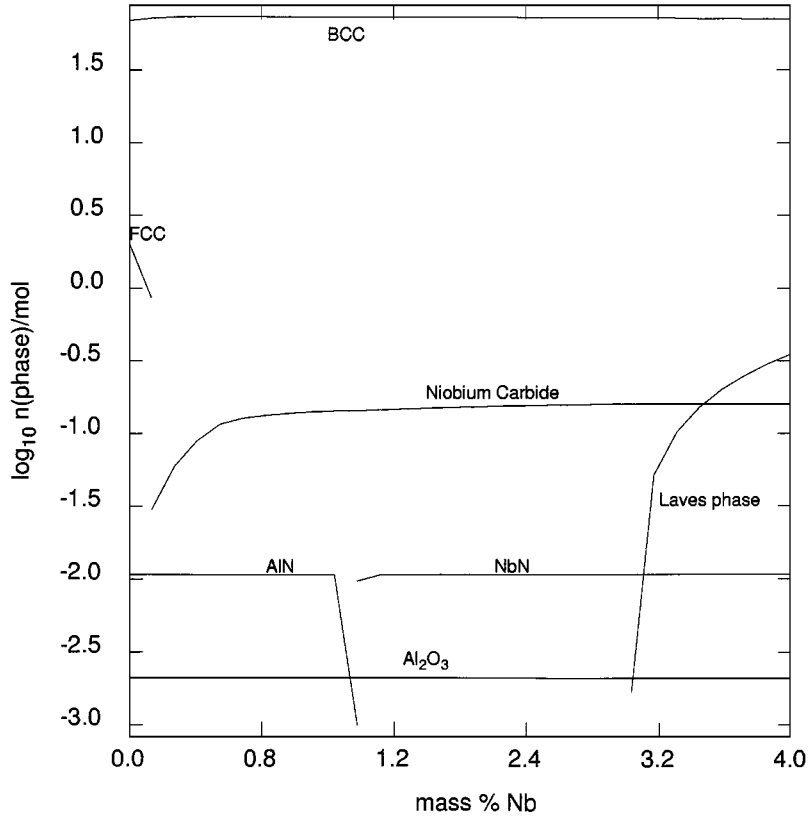

Figure 10 The amounts of phase present as predicted by thermodynamic calculation, in an alloy based on the composition S3, but the Nb content varying from 0 to 4 wt%.

system but is metastable with slow cooling rates [10, 11]. The phase found in the steel S1 was found to contain about 30 Fe, 67 Nb and 4 Si (wt%), showing strong partitioning of Si to the Fe_2Nb_3 phase (Table III). Even in the lower Si containing steel (S4), a small amount of Si was detected in this type of particle. However, the η-Fe_2Nb_3 phase was not detected in the two higher Al containing steels. This result suggests that it is Si not Al that has a stabilising effect on the η-Fe_2Nb_3 phase.

Thermodynamic calculations were made using the MTDATA [12] suite of programs and thermodynamic data recommended by the SGTE [13] supplemented by data taken from the literature [14, 15]. Because of the limitations of the database only Fe and Nb were allowed in the Laves phase. Thermodynamic data for the Fe_2Nb_3 phase was not available either, and hence it wasn't possible to predict the precipitation of this phase. A series of calculations were made for an alloy with a composition equivalent to alloy S3 at 850°C but with Nb contents between 0 and 4 wt% (Fig. 10). It was found that the bcc-phase, NbC and AlN were present at low Nb levels, the NbN phase being precipitated in preference to AlN at levels above about 1.2 wt% Nb. The Laves phase wasn't predicted to precipitate until the level of Nb was about 3 wt%. The preferential precipitation of NbC is consistent with experiment. However with Al additions, the Laves phase was observed when the Nb content of the material was 0.9 wt%. This suggests that Al accelerates the formation of the Laves phase, but without it being incorporated within the precipitate.

The enthalpies of mixing for Al-Sn alloys (Fig. 11) calculated from thermodynamic data are positive indicating the presence of a metastable miscibility gap at lower temperatures. On the other hand, the enthalpies of mixing of the liquid phase in the Fe-Al system is large and negative. If the enthalpy of mixing curve can be taken as representative of the mutual attraction between the pairs of elements, the implication is that it is energetically more favourable for Al to be in an Fe-environment rather than in the presence of Sn. On the other hand, the enthalpies of mixing of Nb-Sn alloys have been estimated to be more negative than Al-Sn [16, 17] indicating attraction between these two elements. If this concept is then extended to the solid state it can be envisaged that there will be an attraction between the Nb and Sn atoms and a repulsion between the Al and Sn. This encourages the formation of the Laves phase, even though following thermodynamic calculations as shown above, the Laves phase would not be expected to precipitate at the level of Nb used in the experiments. It is the interaction between the Sn and Al which then leads to the stabilisation of the Laves phase by Sn.

It has been noted that Si is enriched in both the Fe_2Nb-Laves phase and the η-Fe_2Nb_3 phase while Sn was only dissolved in the Fe_2Nb-Laves phase by substitutional solution. The relative stability of both types of phases is mainly determined by the size difference of closely packing atoms. The Fe_2Nb Laves phase has the C14 $MgZn_2$ (A_2B)-type crystal structure and the ratio of the Goldschmidt atomic radii of the pure elements forming the $MgZn_2$-type phases (R_B/R_A) varies from 1.05 to 1.40 [18]. The η-Fe_2Nb_3 intermetallic phase, first reported by Goldschmidt [19], is f.c.c. of the prototype Ti_2Ni (A_2B) and in all of these types of compounds the average value of the radius ratio R_A/R_B

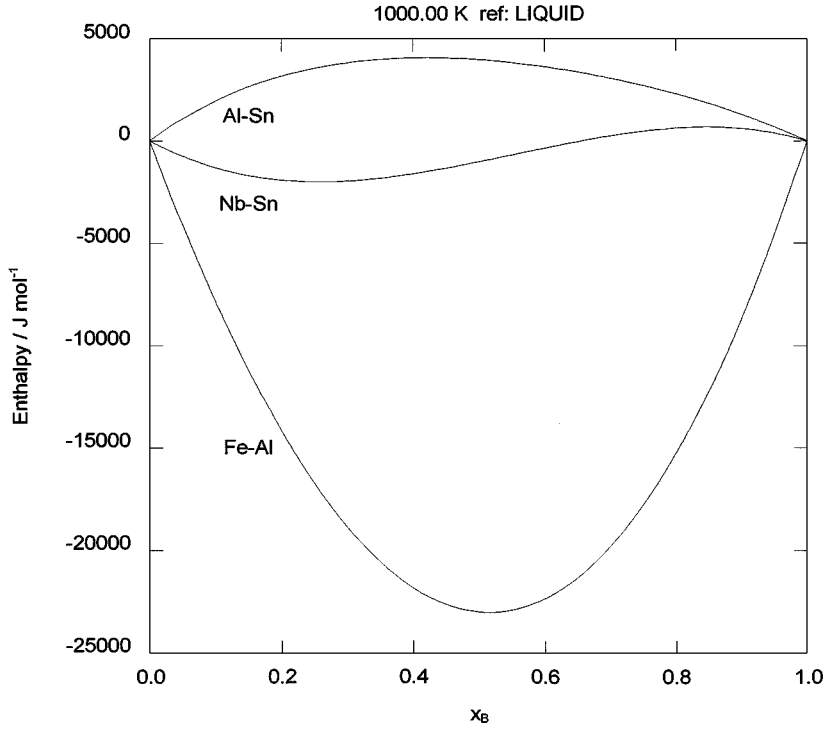

Figure 11 Enthalpy of mixing curves for binary liquids Fe-Al [13], Nb-Sn [16] and Al-Sn [13].

TABLE IV Lattice Spacings (a) and Goldschmidt atomic diameters (d) of the Fe, Nb, Si and Sn elements

Elements	Crystal structure	a (nm) [20]	d (nm) (calculated)
Fe	bcc (α)	0.248	0.256
Nb	bcc	0.286	0.294
Si	diamond	0.235	0.263
Sn	diamond	0.281	0.315

for the binary phase is 1.19 [18]. For individual compounds, the values do not deviate from the average by more than 6% giving a range of 1.12–1.26. The Goldschmidt atomic diameters for Fe, Nb, Sn and Si are calculated according to the crystal structure of the pure elements [20] and are listed in Table IV.

From these values, we can obtain the ratios of the Goldschmidt atomic diameters for Fe, Nb and Si which are $d(\mathrm{Si})/d(\mathrm{Fe}) \approx 1.03$, $d(\mathrm{Nb})/d(\mathrm{Si}) \approx 1.12$. The ratio of $d(\mathrm{Si})/d(\mathrm{Fe}) = (1.03)$ is outside the range for the formation of the Laves phase. Therefore, if Si is dissolved in the Fe_2Nb Laves phase, Si atoms would be expected to replace Fe due to their similar atomic size therefore producing less strain in the lattice than Si substituting for Nb. This can be seen from Table III and Fig. 12a that the Fe content of the Laves phase in alloy S2 (higher in Si) is less than that in alloy S3 (lower in Si), suggesting Si additions replace Fe in the Fe_2Nb-Laves phase. The present results confirm the work of Singh and Gupta [21] and Bardos *et al.* [22]. Similar arguments suggest that Si additions would also replace Fe in the η-Fe_2Nb_3 phase resulting in the lower Fe content of the η-Fe_2Nb_3 phase in the higher Si alloy S1 (30 wt%) than that in the lower Si alloy S4 (37 wt%), as shown in Fig. 12a.

The Goldschmidt atomic diameters for Fe, Nb and Sn give the atomic size ratios of $d(\mathrm{Nb})/d(\mathrm{Fe}) \approx 1.15$, $d(\mathrm{Sn})/d(\mathrm{Fe}) \approx 1.23$ and $d(\mathrm{Nb})/d(\mathrm{Sn}) \approx 0.93$. Therefore, introducing Sn into the Fe_2Nb Laves phase would result in Sn substitution for Nb. From Table III and Fig. 12a, it can be seen that the Nb content of the Laves

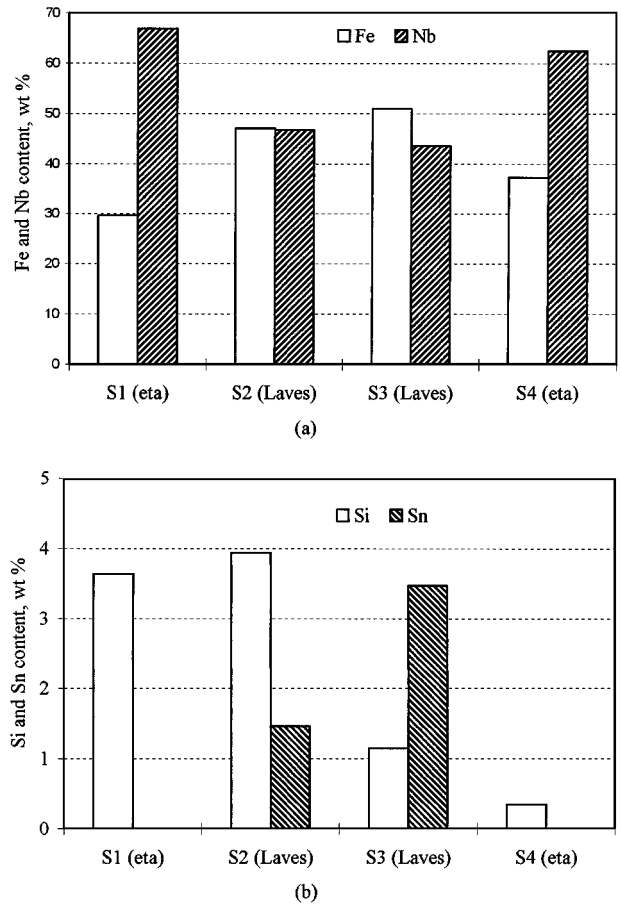

Figure 12 The compositions of η-Fe_2Nb_3 and Fe_2Nb-Laves phases: (a) Fe and Nb content and (b) Si and Sn content.

phase in the lower Si alloy S3 (~44 wt % Nb) is less than that in the higher Si alloy S2 (47 wt% Nb). As Si additions replace Fe in the Laves phase, this suggests that Sn atoms would replace Nb in the Fe_2Nb Laves phase, rather than Fe.

In the η-Fe_2Nb_3 phase, atomic size conditions require that Sn could only replace Nb within the η-Fe_2Nb_3 structure. However, Sn is not detected in the η-Fe_2Nb_3 phase. This result indicates that size factor considerations alone are inadequate to explain the phenomenon found here. Other effects such as crystal structure and atomic ordering arrangements of the phases involved should be considered as these are also important factors affecting the formation and the stability of alloys phases. For example, in the hexagonal Fe_2Nb Laves phase, the large Nb atoms occupy the coordination number (CN) 16 sites with 4 Nb atoms and 12 Fe atoms as neighbours. The packing of the two sets of atoms is such that only like atoms are in contact. In the f.c.c. η-Fe_2Nb_3 phase, as its composition deviates from A_2B stoichiometry, the atomic ordering arrangements of Nb and Fe are not clear. In its prototype, Ti_2Ni, the larger atoms (Ti) occupy two different coordination number sites. The CN 12 sites have an equal number of Ti and Ni neighbours, and the CN 14 sites, have 10 Ti and 4 Ni neighbours. We would expect Nb in η-phase to behave like Ti. If this is the case, Nb in the η-phase would have a different coordination number to that in the Laves phase. These differences in coordination number may result in the ability for Sn to replace Nb atoms in the Fe_2Nb Laves phase but not in the η-Fe_2Nb_3 phase.

By comparing the compositions of the precipitates in alloys containing the same levels of Si, i.e. steels S1 and S2 which contain about 0.3 wt% Si and steels S3 and S4 which contain about 0.02 wt% Si, it seems that the Laves phase dissolves more Si than the corresponding η-Fe_2Nb_3 phase (Table III and Fig. 12b). This is consistent with the work of Goldschmidt [19]. It has been noted that the amounts of Sn dissolved in the Laves phase for steel S3 is higher than that in steel S2 (Fig. 12b) which dissolved a higher amount of Si. This reflects the limited solubility of the third element in the Laves phase, which may be due to electronic concentration requirements as both Si and Sn are in group (IV_B) of periodic table.

The concept of size factor in determining phase stability is not new [20] but it would appear from this study that ternary additions can modify the stability of intermetallic phases in a consistent way. Hence, the solubility of Sn in the Fe_2Nb Laves phase can be understood in terms of atomic size and co-ordination number considerations. There is also the strong suggestion that where no mutual interaction exists between two elements, eg Al-Sn, the use of in this case Al, can displace Sn from the matrix or grain boundary sites hence offering a new strategy for dealing with Sn segregation.

5. Conclusions

The microstructures of the precipitates in low carbon steels with Sn additions have been characterised and the effects of Al and Si on the Sn-precipitation have been discussed. The most important conclusions from this study are as follows:

1. The precipitates found in the four low carbon steels after ageing at 1150°C and 850°C comprise AlN, NbC, η-Fe_2Nb_3 phase and Fe_2Nb-Laves phase.
2. In the lower Al and Al free steels aged at 850°C, the metastable η-Fe_2Nb_3 phase has been observed which dissolves Si replacing Fe.
3. In the higher Al steels aged at 850°C, the Fe_2Nb-Laves phase was found to dissolve both Si and Sn. Si additions replace Fe, and Sn replaces Nb. The Laves phase has a limited solubility for the third element.
4. A concept based on size factor and atomic interactions revealed by study of binary thermodynamic quantities has been used to explain experimental observations.

Acknowledgements

This work was supported by EPSRC Research Grant GR/L38639. The authors also would like to thank Dr. Eric Condliffe, for help with the electron probe microanalysis, and the National Physical Laboratory, Teddington, UK for the provision of the MTDATA software.

References

1. K. NORO, M. TAKEUCHI and Y. MIZUKAMI, *ISIJ International* **37** (1997) 198.
2. J. J. MOORE, *Int. Met. Rev.* **23** (1978) 241.
3. J. PEACE, in "Recycling of Scrap for High quality Products" (ECSC Agreement Number: 7210.CB/815, Draft Final Report, British Steel plc, 9 Albert Embankment, London, February 1998) to be published in Steel Research.
4. T. B. MASSALSKI, P. R. SUBRAMANIAN, H. OKAMOTO and L. KACPRZAK, "Binary Alloy Phase Diagrams," 2nd ed. (ASM, Metals Park, Ohio, 1990) p. 111, 1083 and 1117.
5. X. LI, A. WATSON, R. BRYDSON, A. JHA and R. C. COCHRANE, *Mater. Sci. Tech.* **15** (1999) 1001.
6. P. VILLARS and L. D. CALVERT, "Pearson's Handbook of Crystallographic Data for Intermetallic Phases, Vol. 2" (American Society for Metals, Metals Park, OH 44073, USA, 1985) p. 1031 and 1559.
7. V. RAGHAVAN, "Phase Diagram of Ternary Iron Alloys, Part 1" (Indian Institute of Technology, Delhi, 1987) p. 3.
8. T. TAKASUGI and M. YOSHIDA, *J. Mater. Res.* **13** (1998) 2505.
9. T. GLADMAN, "The Physical metallurgy of microalloyed steels" (The Institute of Materials, London, 1997) p. 88.
10. J. M. Z. BEJARANO, S. GAMA, C. A. RIBEIRO, G. EFFENBERG and C. SANTOS, *Z. Metallkd* **82** (1991) 615.
11. J. M. Z. BEJARANO, S. GAMA, C. A. RIBEIRO and G. EFFENBERG, *ibid.* **84** (1993) 160.
12. R. H. DAVIES, A. T. DINSDALE, T. G. CHART, T. I. BARRY and M. H. RAND, *High Temp. Sci.* **26** (1990) 251.
13. I. ANSARA and B. SUNDMAN, "Computer Handling and Dissemination of Data" (Report CODATA, 1987) p. 154.
14. G. C. COELHO, S. G. FRIES, H. L. LUKAS, P. MAJEWSKI, J .M. Z. BEJARANO, S. GAMA, C. A. RIBEIRO and G. EFFENBERG, in the Proceedings of the Klaus Schultze Symposium on Processing and Applications of High Purity Refractory Metals and Alloys, Pittsburgh, Penn. USA, Oct. 1993, 51.
15. K. C. HARI KUMAR, P. WOLLANTS and L. DELAEY, *CALPHAD* **20** (1996) 139.
16. A. WATSON, unpublished work.

17. F. R. DE BOER, R. BOOM, W. C. M. MATTENS, A. R. MIEDEMA and A. K. NIESSEN, "Cohesion and Structure—Vol. 1, Cohesion in Metals, Transition Metal Alloys" (Elsevier, Amsterdam 1988) p. 396.
18. M. V. NEVITT, in Symposium on Electron Structure and Alloy Chemistry of the Transition Elements, New York, February 22, 1962, edited by P. A. Beck (American Institute of Mining, Metallurgical, and Petroleum Engineers, Inc. 1963) p. 127.
19. H. J. GOLDSCHMIDT, *J. Iron and Steel Inst.* **194** (1960) 169.
20. R. E. SMALLMAN, W. HUME-ROTHERY and C. W. HAWORTH, "The Structure of Metals and Alloys" (The Institute of Metals, London, 1969) p. 104.
21. B. N. SINGH and K. P. GUPTA, *Metall. Trans.* **3** (1972) 1427.
22. A. M. BARDOS, D. I. BARDOS and P. A. PECK, *Trans. Met. Soc. AIME* **227** (1963) 991.

Received 28 July
and accepted 19 August 1999